J. Fluid Mech. (1987), *vol.* 185, *pp.* 385–414
Printed in Great Britain

Wave splitting in a fluid of large heat capacity

By PHILIP A. THOMPSON,
Rensselaer Polytechnic Institute, Troy, NY 12180-3590, USA

HUMBERTO CHAVES, G. E. A. MEIER,
Max-Planck-Institut für Strömungsforschung, D3400 Göttingen, Federal Republic of Germany

YOON-GON KIM
Rensselaer Polytechnic Institute, Troy, NY 12180-3590, USA

AND H.-D. SPECKMANN
Deutsche Forschungs- und Versuchsanstalt für Luft- und Raumfahrt (DFVLR), D3400 Göttingen, Federal Republic of Germany

(Received 17 September 1986 and in revised form 25 May 1987)

The splitting of a single pressure discontinuity into a propagating two-wave system is studied for the case of saturated-liquid expansion (liquid-evaporation wave splitting) and vapour compression (vapour-condensation wave splitting). Experimental results from the Max-Planck-Institut für Strömungsforschung and from Rensselaer Polytechnic Institute show that splitting occurs in test fluids of large molar heat capacity, such as iso-octane ($C_v^0/R \approx 37$). Each of the two forms of splitting results in a single-phase forerunner wave carrying a pressure discontinuity followed by a phase-change wave, also with a pressure discontinuity. The thermodynamic state between the forerunner wave and the phase-change wave is metastable (supersaturated liquid or vapour). The waves are quantitatively described by systems of adiabats, e.g. shock adiabats. It appears that nucleation processes are predominantly homogeneous.

In vapour-compression shock-wave splitting, a combined wave (liquefaction shock) splits into discrete forerunner and condensation waves at a triple point, the intersection of a liquefaction shockfront, forerunner shock and condensation discontinuity: such a point occurs just at critical supersaturation (i.e. the Wilson-line state), where condensation is spontaneous and immediate. For shock waves that produce a metastable state of subcritical supersaturation, condensation is delayed, that is, the condensation discontinuity propagates more slowly; for a split-shock system, the condensation discontinuity propagates subsonically. The pressure amplitude of a real split-shock system is much larger than that predicted by an equilibrium model.

In liquid-evaporation wave splitting, the forerunner wave is an acoustic expansion wave and the second wave an evaporation wave with a propagation velocity approximately determined by the Chapman–Jouguet condition for deflagration. Such evaporation wavefronts are increasingly distinct as the temperature approaches the critical-point value. The evaporation rates across the wavefront are comparable to those found in vapour explosions.

1. Introduction

Rapid, wave-induced adiabatic phase changes occur in fluids of high molar heat capacity, such as octane (adiabatic phase changes in fluids of low molar heat capacity, such as water, are different in kind). Much of the physical and historical background for these phenomena is surveyed in a preceding paper (Thompson, Carofano & Kim 1986, hereinafter referred to as Φ ($\Phi\alpha\sigma\iota\delta$ = phasis = phase)). The present work is a continuation of Φ.

The term *wave splitting* of the title is intended to mean a system of two longitudinal waves: the first and normally faster wave is a pressure discontinuity and the second wave is a phase and pressure discontinuity. The two-wave system can evolve from a single, combined wave which splits into two parts. This description represents a modest extension of the term *shock splitting* (Zel'dovich & Raizer 1967; Bethe 1942; Thompson & Kim 1983). Two cases of adiabatic wave splitting are treated in this paper: vapour condensation and liquid evaporation. The terminology is summarized in table 1.

Shock splitting associated with vapour condensation has been the subject of experiments reported by Dettleff *et al.* (1982), by Thompson & Kim (1983), Thompson, Kim & Meier (1984) and by Speckmann (1984). The liquid-evaporation wave splitting has been described by Chaves (1984). Shock splitting associated with solid–solid phase transitions is described by Zel'dovich & Raizer in general terms and by many authors for particular phase transitions: for the graphite → diamond transition, data are given by McQueen & Marsh (1968) and by Gust & Young (1979). Ordinary Mach reflection of a shock wave may be regarded as a form of shock splitting, in the sense that an incident wave 'splits' into a reflected wave and a Mach stem. This wave pattern depends on the reflection boundary condition for its existence, however, rather than an interaction between the wave and the medium, as in the phenomena listed in table 1.

We thus choose to restrict the term 'wave splitting' to phenomena that can occur even in one-dimensional flows. Shock splitting – into a shock wave and an ionization wave – is believed to occur in nebulae and to play a role in star formation (Mihalas & Mihalas 1984); this type of splitting has been observed in the laboratory (Wong & Bershader 1966; Smith 1968). A shock wave in the vapour of low-temperature helium will split upon reaching the liquid surface (superfluid) into a two-wave system: the 'first-sound' wave and the 'second-sound' wave (Liepmann & Laguna 1984). Certain forms of cavitation, including 'column separation' appear to represent wave splitting. Consideration of wave splitting in ship waves may even be of interest.

One-dimensional wave splitting for both the liquid-evaporation and vapour-condensation cases is shown schematically for one-dimensional flow in figure 1. The initial fluid states are those at the right-hand ends, i.e. liquid and vapour, respectively. The wave and fluid motion is initiated by a driving piston, as in conventional one-dimensional gasdynamics. For uniform initial states, the waves may be considered to be simple with all waves travelling to the right.

In their most elementary forms, both cases of wave splitting shown in figure 1 can be explained simply by the difference between the single-phase sound speed C_f and the mixture of sound speed C_m. As discussed in detail in Φ, $C_f \geqslant C_m$ at both the saturated-liquid phase boundary and the saturated-vapour boundary. Under the assumption of equilibrium states and small-amplitude (acoustic) waves, both the forerunner wave FW and the forerunner shock wave FS propagate with their respective single-phase sound speeds and both phase-discontinuity waves EW and

Wave process	Liquid evaporation Liquid-side wave splitting	Vapour condensation Vapour-side shock splitting
First wave	Forerunner wave $[P] < 0, \quad M \approx 1$ (acoustic) liquid → supersaturated liquid	Forerunner shock $[P] > 0, \quad M > 1$ vapour → supersaturated vapour
Second wave	Evaporation wave $[P] < 0, \quad M < 1$ supersaturated liquid → mixture	Condensation discontinuity $[P] \geqslant 0, \quad M < 1$ supersaturated vapour → mixture
Combined wave	Complete evaporation shock (hypothetical)	Liquefaction shock $[P] > 0, \quad M > 1$

TABLE 1. Split-wave, liquid–vapour systems. The Mach number M of the wave discontinuity refers to the velocity of the discontinuity with respect to the fluid ahead, divided by the sound speed of that fluid. The states referred to correspond to the real, non equilibrium case of wave splitting.

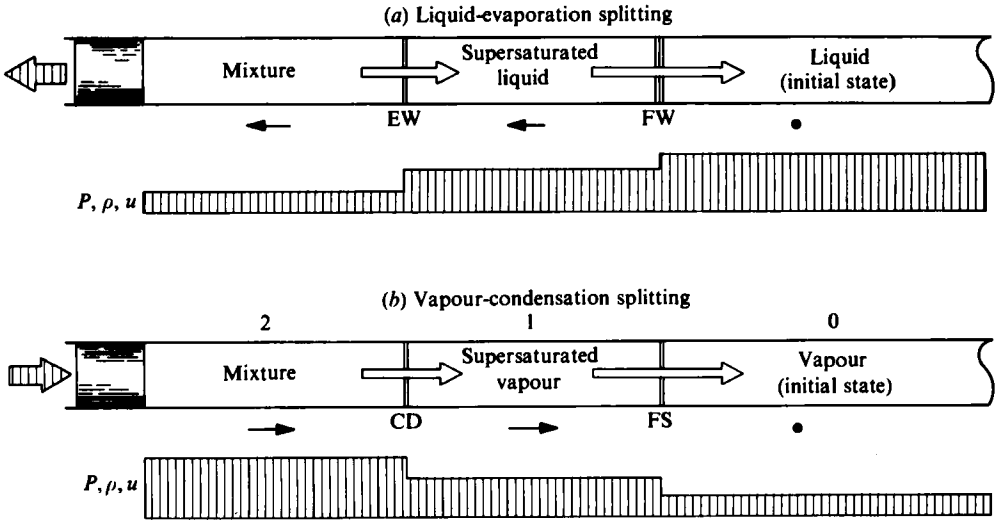

FIGURE 1. Conceptual representation of one-dimensional wave splitting in a liquid–vapour system. All waves are travelling to the right. Direction of the impulsive piston motion is indicated by broad-banded arrows, fluid motion by the thin black arrows. (*a*) Rarefaction wave leading to liquid-evaporation splitting. FW = forerunner wave, EW = evaporation wave. (*b*) Compression wave leading to vapour-condensation splitting. FS = forerunner shock, CD = condensation discontinuity.

CD propagate with their respective mixture sound speeds. Because the single-phase sound speed is greater in both cases, the forerunner wave will run ahead of the phase-discontinuity wave, i.e. wave splitting will occur. In the equilibrium case, the fluid state between the forerunner wave and the phase discontinuity will be just saturated (see, e.g. Bethe 1942).

The difference between the single-phase sound speed C_{f} and the mixture sound speed C_{m} is expressed at the saturation boundary by the 'kink' k in Φ by

$$k \equiv \frac{C_{\mathrm{f}}^2 - C_{\mathrm{m}}^2}{C_{\mathrm{m}}^2} = -\frac{T}{C_v}\left(\frac{\partial P}{\partial v}\right)_T \left(\frac{\mathrm{d}s}{\mathrm{d}P}\right)_\sigma^2, \tag{1}$$

where partial derivatives refer to the single-phase value and the subscript σ refers to a derivative along the liquid or vapour saturation boundary. On the liquid side L, $(\mathrm{d}s/\mathrm{d}P)_\sigma > 0$ and $C_{\mathrm{fl}} > C_{\mathrm{ml}}$: thus, the condition for wave splitting in a weak expansion wave is always formally fulfilled. (This result should be treated with caution, however, if only because the extremely low values of C_{ml} predicted from equilibrium thermodynamics cannot be physically realized in laboratory-scale systems). On the vapour side V, $(\mathrm{d}s/\mathrm{d}P)_\sigma^2 \geqslant 0$ and $C_{\mathrm{fv}} \geqslant C_{\mathrm{mv}}$. In order for shock splitting to take place, $C_{\mathrm{fv}} \geqslant C_{\mathrm{mv}}$. For shock splitting to be realized, however, it is necessary that adiabatic compression lead to vapour condensation. This is the retrograde property discussed in Φ and will be fulfilled if the 'retrogradicity' r satisfies

$$r \equiv \left(\frac{\partial T}{\partial v}\right)_p \left(\frac{\mathrm{d}s}{\mathrm{d}P}\right)_\sigma > 0 \tag{2}$$

on the saturated-vapour boundary. It is not difficult to show that (2) can be fulfilled by substances with large molar heat capacities. We remark that the kink k and retrogradicity r are related by

$$\frac{k}{r^2} = \gamma - 1, \tag{3}$$

where γ is the ratio of specific heats.

In summary, the elementary conditions for equilibrium-state expansion-wave splitting are satisfied in principle on the liquid side, independent of heat capacity, for all real fluids. On the vapour side, the conditions for equilibrium-state compression-wave splitting are satisfied for a fluid of large heat capacity (the results discussed in this paper pertain only to large-heat-capacity fluids). As discussed in the following, however, both forms of splitting are found experimentally to produce metastable (super-saturated) states behind the forerunner pressure wave and the equilibrium-state model does not yield realistic quantitative results. The observed wave splitting is essentially coupled with non-equilibrium effects.

As in Φ, the characteristic heat capacity of a given fluid is represented by

$$\tilde{C}_v \equiv \frac{C_v^0(T_{\mathrm{c}})}{R} \tag{4}$$

which represents the ideal-gas, constant-volume heat capacity at the critical temperature.

The isentropes and saturation boundaries shown in figure 2 were calculated from the Hobbs equation of state (Hobbs 1983). This equation is constrained to yield isotherms which have the form of van der Waals (cubic) isotherms over the entire range of states – stable, metastable and unstable, including negative-pressure states – so that there are just two spinodal lines. In addition, experimental data for metastable states of *n*-hexane (Ermakov & Skripov 1968) are included in the data base. There is thus reason to expect that the metastable states may be realistically calculated.

It is convenient to illustrate both forms of wave splitting with the diagrams in figure 2, noting, however, that there is no causal connection between these two separate phenomena.

Liquid-evaporation splitting can originate from an initial compressed-liquid state on the isentrope above point h in figure 2(*a*). If the pressure is released, for example by piston withdrawal or diaphragm burst, a system of waves similar to those in figure

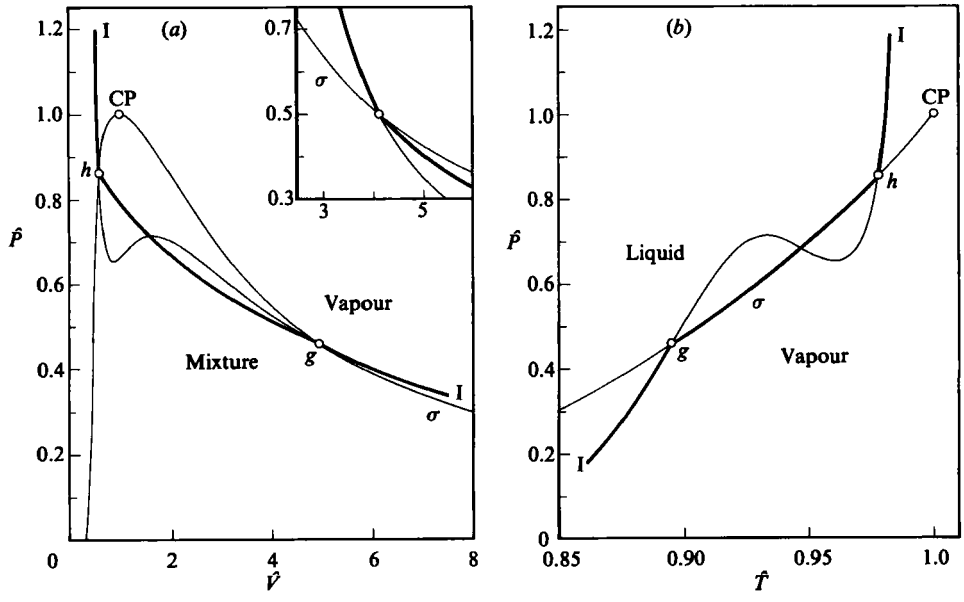

FIGURE 2. Equilibrium isentropes (heavy lines) and non-equilibrium isentropes (lighter lines) for perfluoro-*n*-hexane C_6F_{14} ($\tilde{C}_v = 40.5$). σ = saturation boundary. The single isentrope shown has an entropy $(S-S_c)/R = -2.07$, where S_c is the critical value. (*a*) Pressure–volume diagram in reduced coordinates. (Inset: isentrope for argon, with $\tilde{C}_v = 1.5$, near the saturated-vapour boundary.) (*b*) Pressure–temperature diagram in reduced coordinates.

1(*a*) would evolve. Ideally, the successive states (compressed liquid, saturated liquid and mixture) would follow the isentrope downwards, as a sequence of equilibrium states. For the typically rapid processes of interest here, however, the expanding liquid passes through the saturation pressure at point *h* without a phase change, that is, becomes supersaturated, following the non-equilibrium branch of the isentrope downwards. The increasing supersaturation is terminated when the nucleation rate in the liquid becomes sufficiently high: in an extremely rapid expansion, this state may approach the liquid spinodal. In this real, non-equilibrium case, the propagation velocity of the forerunner wave FW is still approximately the speed of sound in the liquid. The propagation velocity of the evaporation wave EW can no longer be the mixture sound speed C_{ml} at the kink, however, since the corresponding thermodynamic state has been exceeded without any phase change. The determination of this propagation velocity will be addressed in §3.

Vapour-condensation splitting can originate from an initial superheated-vapour state on the isentrope below point *g* in figure 2(*a*). Sudden compression, for example by piston advance or diaphragm burst, will produce a compression shock wave, the forerunner shock (for qualitative discussion, we consider the shock adiabat to be identical with the isentrope). If the compression is sufficiently strong, vapour condensation will occur. Just as in the liquid-evaporation case, however, the phase change is delayed and the vapour passes through the saturation pressure at point *g* without a phase change and becomes supersaturated. The increasing supersaturation along the non-equilibrium isentrope (or shock adiabat in the real, nonlinear case) is terminated by an abrupt condensation when the droplet nucleation rate reaches a sufficiently high value corresponding to critical supersaturation, or in engineering terminology, the Wilson line. The concept of a fixed critical-supersaturation limit

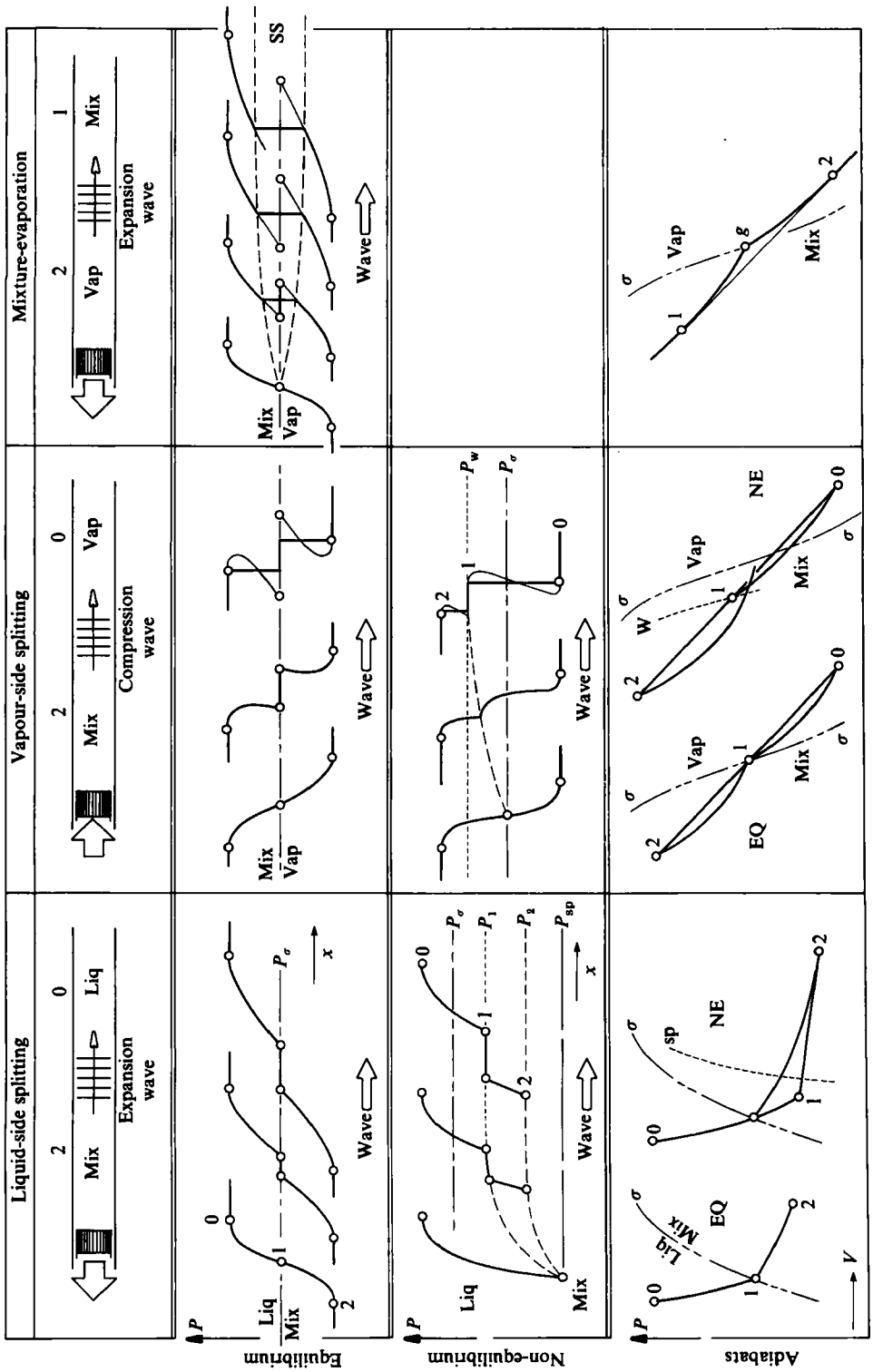

FIGURE 3. Nonlinear wave evolution, steepening and splitting, with pressure–volume adiabats, for liquid-evaporation wave splitting, vapour-condensation shock splitting and mixture-evaporation (rarefaction) shocks. NE = non-equilibrium, EQ = equilibrium, P_σ = saturation pressure, P_{sp} = spinodal pressure, W = Wilson line, SS = sonic–sonic (Chapman–Jouguet) shock.

corresponds to an extremely steep increase in nucleation rate with increasing supersaturation. It represents a simplification that omits physical processes which could be important; its validity may be inferred from the extent to which an experimental Wilson line, representing the onset of nucleation, is found to be a fixed line independent of the rate of supersaturation (see, among others, Wegener & Wu 1977; Dobbins 1983).

The forerunner shock propagates at a velocity of the order of the single-phase sound speed (more precisely, at the velocity $M_s C_f$, where M_s is the forerunner-shock Mach number). The propagation velocity of the following condensation discontinuity CD will be discussed in §2.

The splitting of a pressure wave has been described thus far for waves of limited amplitude, beginning from the very small-amplitude acoustic case. For very large pressure amplitudes, however, the phase-change wave (e.g. the condensation discontinuity CD) can actually overtake the forerunner wave, resulting in a single, combined wavefront as listed in table 1. In the case of the liquefaction shock (the combined wave corresponding to vapour condensation), the existence and behaviour of the combined wave is well documented (Dettleff *et al.* 1979; Thompson *et al.* 1984; *Φ*). The upstream state for a liquefaction shock is typically superheated vapour; the downstream state can be mixture or, in the case of strong shocks, compressed liquid (corresponding to complete liquefactions). The weakening of a liquefaction shock will result in shock splitting (Thompson & Kim 1983): this form of splitting will be discussed in §2.

Other phenomena associated with phase-boundary crossings are briefly described by Meier & Thompson (1985) for both regular and retrograde behaviour. One additional phenomenon, the development of the mixture-evaporation shock, is depicted in figure 3, along with equilibrium and non-equilibrium forms of wave splitting (additional information on the mixture-evaporation shock is given in *Φ*). It is remarkable that the mixture-evaporation (rarefaction) shock is the reversed form of a vapour-condensation or weak liquefaction shock, but cannot split: the development of the discontinuity is governed by the effective negative nonlinearity at the kink g, leading to a sonic–sonic rarefaction shock (see the corresponding adiabat in figure 3).

The classical wave steepening depicted in figure 3 assumes that the nonlinearity parameter Γ (fundamental derivative) is locally positive and (in the equilibrium cases) that the sound speed is discontinuous at the saturation boundary as discussed above. Certain features of the construction are hypothetical, in particular, the near-spinodal minimum pressure for non-equilibrium liquid-evaporation wave splitting.

2. Vapour-condensation shock splitting and liquefaction shocks

The experiments described here may be considered to be of two kinds. In the first, performed at Rensselaer Polytechnic Institute (RPI), shock splitting is observed when a single liquefaction shock is sufficiently weakened by diffraction or spatial expansion that condensation is delayed and the liquefaction shock front splits into a forerunner shock and a following condensation discontinuity. This may be considered the 'strong' version of shock splitting, because it originates from a wave of higher pressure amplitude. In the second kind of experiment, performed at the Max-Planck-Institut für Strömungsforschung (MPI), shock splitting occurs in many cases in a small-amplitude pressure wave for which critical supersaturation is not

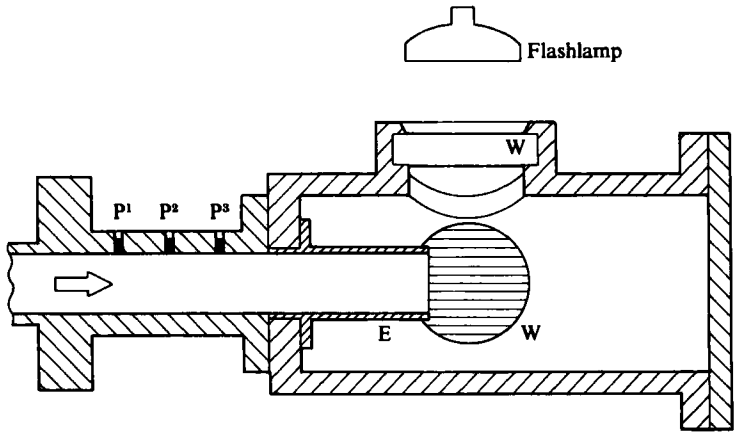

FIGURE 4. Observation chamber at the end of the Rensselaer shock-tube test section. P^1, P^2 and P^3 are pressure transducers, W = window, E = end of the constant-diameter test section. The arrow shows the propagation direction of the incident shock. After *Φ*.

achieved and no combined wave is formed. This may be considered the 'weak' version of shock splitting.

In all experiments, the pressure amplitude ΔP of the condensation discontinuity CD is small compared to that of the forerunner shock FS: typically, $\Delta P_{CD} < \frac{1}{6}\Delta P_{FS}$. The condensation discontinuity itself is dispersive, i.e. a variety of relaxation mechanisms and sound speeds are present. Combined with the small pressure amplitudes, this suggests an analogy with the 'fully dispersed' waves of Lighthill and Whitham (Lighthill 1956).

2.1. *Shock-splitting experiments at RPI*

Photographic observations and measurements were performed in the shock-tube observation chamber shown in figure 4 (see *Φ* for experimental details, including the properties of the test fluids). The shock-tube inside diameter is 57.6 mm, the driver section is 3.50 m long and the test section 1.67 m long, measured from the diaphragm to the open end. The test section has now been operated at diaphragm-burst pressures up to 100 bars.

The essential measurements consisted of liquefaction-shock veocity U_0, the transducer pressures $P(t)$ and the initial conditions P_0, T_0 and v_0.

A typical experimental photograph is shown in figure 5 (compare figure 9 in *Φ*). The liquefaction shock front LS remains plane until it is overtaken by expansion waves originating at the end E of the shock tube, producing a curved and weakening shock front. Splitting occurs at the triple point TP: It is assumed that the pressure amplitude of the forerunner shock at this point is just sufficient to produce critical supersaturation S_c, i.e. that splitting occurs at the Wilson line. Enlarged photographs of the triple point TP show that the three discontinuities propagate at the same normal velocity (see figure 6). Measurement of this velocity yields a unique value for the critical supersaturation. We define the local supersaturation $S(P,T)$ as

$$S \equiv \frac{P}{P_\sigma(T)} \tag{5}$$

and affix the subscript c to indicate the critical value S_c. A large number of measurements of S_c will determine the Wilson line.

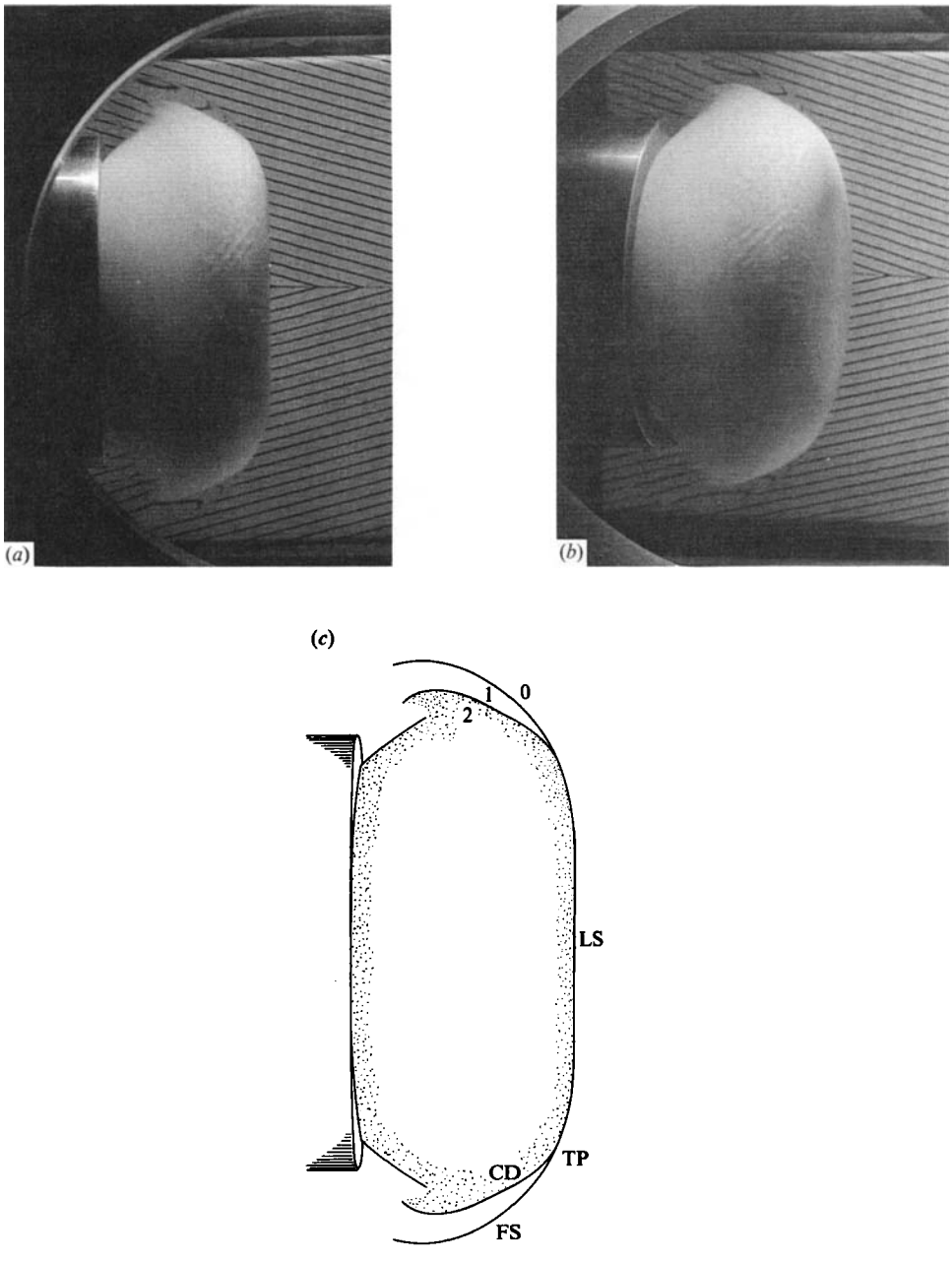

FIGURE 5. Emergence of a liquefaction shock wave in iso-octane into the observation chamber. Flow is from left to right. At the triple point, i.e. TP, the main liquefaction shock LS has split into a curved, vapour-phase forerunner shock FS and a condensation discontinuity CD. Initial conditions $P_0 = 1.10$ bar, $T_0 = 110$ °C. Plane liquefaction-shock Mach number $M_0 = 2.79$. (*a*) Side view. (*b*) Oblique view, showing the plane liquefaction shock front. (*c*) Side-view drawing with terminology. CD = condensation discontinuity, FS = forerunner shock, TP = triple point, LS = liquefaction shock front.

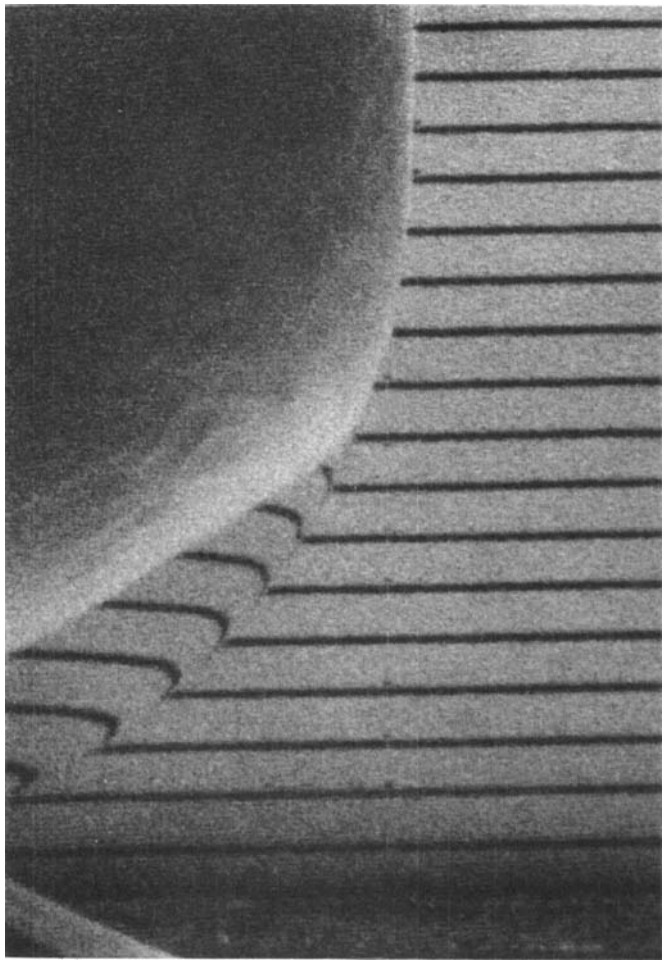

FIGURE 6. Closeup of the triple point in FC-75. Initial conditions $P_0 = 0.95$ bar, $T_0 = 110$ °C. Plane liquefaction shock Mach number $M_0 = 2.04$.

For smaller driving pressures, splitting will occur in the shock-tube test section and the wave system will be globally split on emergence (Thompson *et al.* 1984; Yoon 1985).

Each of the three discontinuities (liquefaction shock, forerunner shock and condensation discontinuity) is described by a Rankine–Hugoniot equation,

$$[h] = \bar{V}[P], \tag{6}$$

where the square brackets denote a jump, i.e. the downstream value minus the upstream value, and $\bar{V}$ denotes the arithmetic average of the upstream and downstream values. Consistent with figure 1, the successive thermodynamic states will be denoted 0, 1, 2:

0 equilibrium superheated vapour: initial state
1 supersaturated vapour (metastable): intermediate state
2 equilibrium mixture: final state

The possible sequences of state are then $0 \rightarrow 1$ (forerunner shock), $1 \rightarrow 2$ (condensation

discontinuity) and $0 \rightarrow 2$ (liquefaction shock). In the case of a strong liquefaction shock, the downstream state 2 could be compressed liquid, but such a case does not occur in the results reported here.

The calculated system of adiabats for the transitions $0 \rightarrow 1$ and $1 \rightarrow 2$, $0 \rightarrow 2$ is shown in figure 7. The special case of a forerunner shock followed by a condensation discontinuity travelling at the same velocity (so that the wavefronts would maintain constant separation in a one-dimensional flow) is shown in (*a*): the equal velocities correspond to the equal slopes of the numbered Rayleigh line $0 \rightarrow 1$ and $1 \rightarrow 2$. If the spatial separation between the two wavefronts is effectively zero, the combined wavefront $0 \rightarrow 2$ represents a single liquefaction shock. That this solution is consistent with the respective Rankine–Hugoniot equations can be formally shown by summing the two equations: in the figure, this corresponds to an intersection of the equilibrium adiabat EA (for liquefaction-shock solutions) with the condensation adiabat CA (for shock-splitting solutions) precisely at point 2. The system of adiabats and Rayleigh lines in figure 7(*a*) thus also represent a triple point, where each of the three waves $0 \rightarrow 1$, $1 \rightarrow 2$ and $0 \rightarrow 2$ travels with the same velocity. For the case illustrated, the triple-point wave velocity $U_{\mathrm{TP}} = M_{\mathrm{FS}} C_0$ is 123 m/s. The corresponding experimental value (run FC75041983-3) is also 123 m/s.

Additional solutions are shown in figure 7(*a*). The Rayleigh line terminating at *l* on the equilibrium adiabat EA represents a liquefaction shock without splitting. The Rayleigh line terminating at *e* on the dry adiabat DA represents a dry shock with a downstream state *e* which has a supersaturation $S < S_{\mathrm{c}}$, i.e. which falls short of the Wilson line. Depending on boundary conditions, this shock may be followed by a delayed condensation discontinuity (the condensation adiabat is not shown, but is readily calculable): splitting from point *e* would represent the weak form of shock splitting.

The shock adiabats in figure 7(*a*) can be compared to the isentropes in the pressure–volume plane of figure 2(*a*). For example, the dry adiabat DA is similar to the non-equilibrium isentrope above point *g* in figure 2(*a*).

Other, less specialized splitting solutions from a common state of critical supersaturation 1 are shown in figure 7(*b*), where the velocity of the condensation discontinuity $1 \rightarrow 2$ (or $1 \rightarrow z$, etc.) can be inferred from the slope of the corresponding Rayleigh line. The cross-hatched area corresponds to impossible solutions with imaginary mass flux through the condensation discontinuity. The transition $1 \rightarrow p$ represents a contact surface, i.e. a condensation discontinuity with propagation velocity zero and no pressure jump. Additional states on the condensation adiabat CA for state 1 correspond to a condensation discontinuity which is falling behind the forerunner shock FS (as at *z*), propagating at just the velocity of the FS (as at 2) and overtaking the FS (as at the uppermost point on CA). Figure 7(*c*) shows the same adiabat system in entropy–volume coordinates, which clearly separate the various adiabats.

There are no Chapman–Jouguet points on the condensation adiabat. This corresponds to the condensation discontinuity CD being an 'endothermic detonation' in the terminology of Hayes (Hayes 1958; Thompson *et al.* 1984) although it actually 'releases' heat by condensation and is somewhat analogous to a flame front. In the observed, compression form of this discontinuity it appears that it propagates subsonically with respect to the supersaturated but still dry vapour 1 ahead, as indicated by the following calculation.

Let U_{FS} and U_{CD} be the velocities of the forerunner shock front and the condensation discontinuity, respectively, and U_1 the velocity of the supersaturated

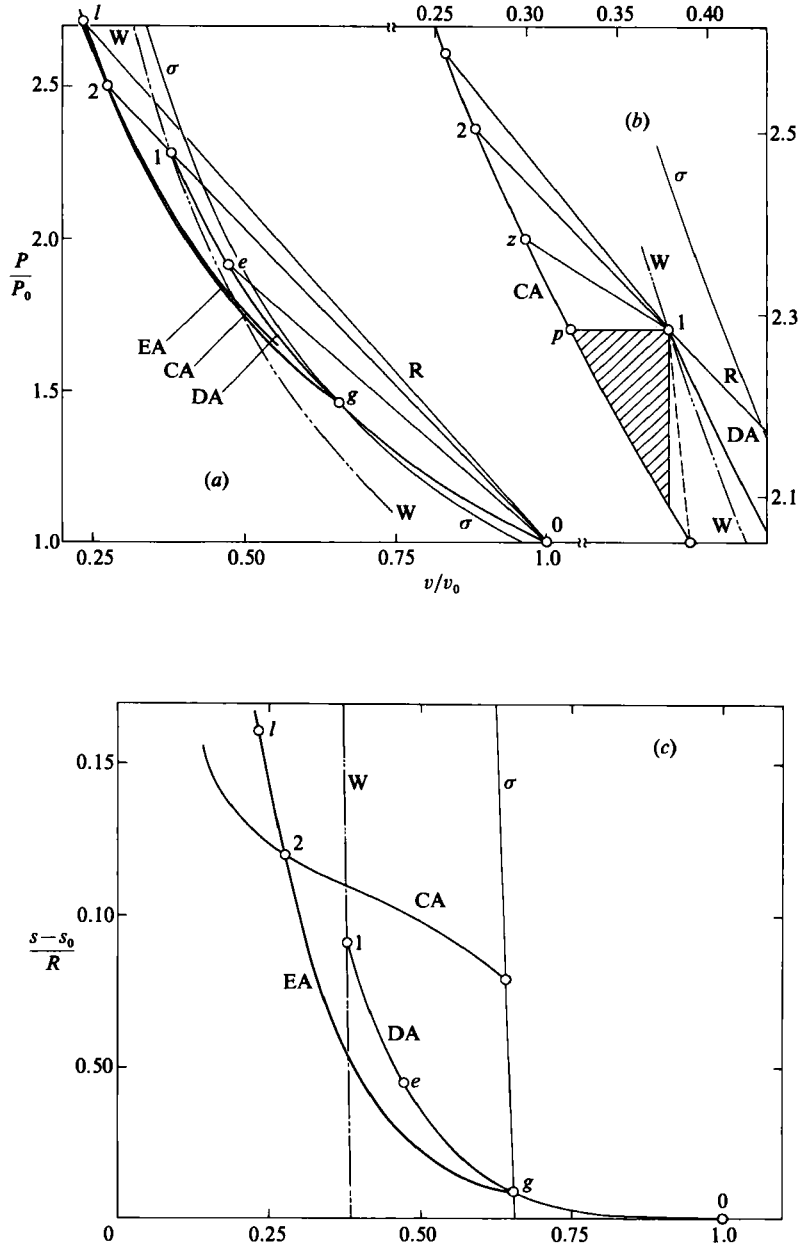

FIGURE 7. The system of shock adiabats for shock splitting in the fluorocarbon FC-75, calculated from the Hobbs equation of state. Forerunner shock Mach number $M_{FS} = 1.497$. Initial conditions $P_0 = 1.80$ bar, $T_0 = 135$ °C, $v_0 = 40.85$ cm^3/g, $C_0 = 82.3$ m/s. (*a*) Adiabats in the pressure–volume plane. EA = equilibrium adiabat, CA = condensation adiabat, DA = dry adiabat (metastable), R = Rayleigh line, σ = saturated vapour boundary, W = Wilson line. (*b*) Enlarged portion of (*a*), showing alternative end states on the condensation adiabat. Dashed line corresponds to a rarefaction (not observed). (*c*) Adiabats in the entropy–volume plane.

vapour 1, all in the laboratory frame. With the shock Mach number M_{CD} of the condensation discontinuity defined in the usual way, i.e. $M_{CD} \equiv W_1/C_1$, where $W_1 = U_{CD} - U_1$ is the velocity of propagation with respect to the fluid ahead, conventional shock relations (e.g. Thompson 1972) yield

$$M_{CD} = M_{FS}\frac{C_0}{C_1}\left[1 - \frac{\delta}{M_{FS}} - \frac{\Pi_{FS}}{M_{FS}^2}\right], \tag{7}$$

where $\delta \equiv (U_{FS} - U_{CD})/C_0$ is the non-dimensional velocity difference between the forerunner shock and the condensation discontinuity, and Π_{FS} is the forerunner shock strength. At the triple point, $\delta = 0$ and (7) becomes, with Π_{FS} written explicitly,

$$M_{CD} = M_{FS}\frac{C_0}{C_1}\left[1 - \frac{P_1 - P_0}{\rho_0 U_0^2}\right]_{\delta=0}. \tag{8}$$

Making use of fast-convergence shock series (Thompson 1983) this reduces to the approximate relation

$$M_{CD} = M_{FS}^{-1} + O(\gamma - 1), \tag{9}$$

where $\gamma - 1$ is ≈ 0.02. This result is based on the assumption that the sound speed C_1 is the single-phase value for the supersaturated vapour. The presence of droplet nucleation ahead of the condensation discontinuity, however, could lower the value of C_1, so that $C_0/C_1 \approx (k+1)^{\frac{1}{2}}$, roughly 1.1 for typical experimental fluids, corresponding to (1). This modification would not alter the conclusion that the condensation discontinuity at the triple point is subsonic. In general, it would appear that the condensation wave is subsonic except in very special circumstances.

A plot of the experimental condensation-discontinuity Mach number M_{CD} against the forerunner-shock Mach number for the special triple-point case described by (8) and (9) is shown in figure 8. For $\delta < 0$, the condensation discontinuity will overtake the forerunner shock and form a liquefaction shock, i.e. the split-shock system no longer exists. The slope of the Rayleigh line $1 \rightarrow 2$ can be related to the propagation velocity w_1 by the discontinuity equation

$$\frac{P_2 - P_1}{V_2 - V_1} = -\rho_1^2 w_1^2 \leqslant 0. \tag{10}$$

Allowable Rayleigh lines are shown in figure 7(*b*), including one dashed line corresponding to a rarefaction (such rarefactions have not been observed, nor do they appear to have physical significance). Note that the range of allowable states 2 on the adiabat CA is restricted by the entropy condition $[s] \geqslant 0$ (see figure 7*c*). All of the possible Rayleigh lines in figure 7(*a*, *b*) for the condensation discontinuity ($1 \rightarrow p$, $1 \rightarrow z$, etc.) correspond to subsonic propagation.

The onset of shock splitting and the amplitude of the waves are essentially fixed by the Wilson line, which must be determined by experiment (except in the – fictitious – equilibrium limit, where the Wilson line is identical with the saturation boundary σ). The experimental data for FC-75, based on triple-point measurements, are shown in figure 9. The fitted curve W is represented by

$$S_c(T) = \exp\left[\alpha \hat{T}^{-4}(\hat{T}^{-\frac{3}{2}} - 1)\right], \tag{11}$$

where $\alpha = 0.467$ and $\hat{T} \equiv T/T_c$ is reduced temperature.

To test the invariance of the fitted Wilson line, a series of experiments was performed with a common, supersaturated target end state 1 on the Wilson line, but

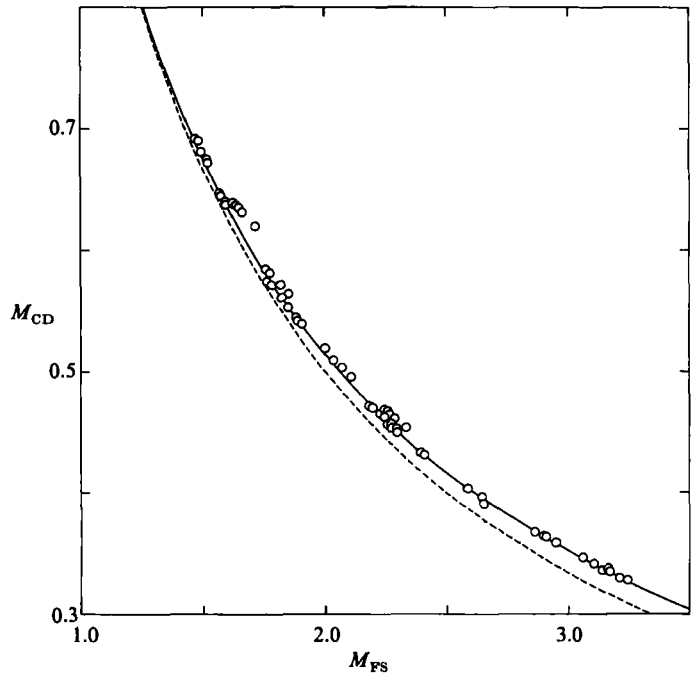

FIGURE 8. Experimental condensation-discontinuity Mach number M_{CD} *vs.* experimental forerunner-shock Mach number M_{FS}, measured at the triple point. The solid curve corresponds to equation (8), the dashed curve to equation (9).

with a variety of initial states 0. An inverse shock adiabat was constructed from the target end state 1 ($T_1 = 122$ °C, $P_1 = 2.61$ bar, $S_c = 1.56$), so that all points on the adiabat represent possible initial states 0 (see figure 10*a*). In various experiments from the defined initial states, the triple-point pressures and temperatures were determined, allowing the calculation of the corresponding S_c, as shown in figure 10(*b*). The values of $S_c (\approx 1.55)$ thus found are approximately independent of liquefaction-shock Mach number M_0 (the slightly lower values of S_c at $T_0 = 85$ °C and 90 °C can be partially attributed to not passing through the target state 1.

The pressure amplitude that can be achieved in a split-shock system, e.g. the value $P_2 - P_0$ in figure 7(*a*), is considerably greater in the real, non-equilibrium case than in the ideal, equilibrium case. A quantitative comparison, shown in figure 11, is based on a triple-point system in each of the two cases, with a common initial state O and a common adiabatic-crossing of the equilibrium saturation boundary σ. The construction of the comparison is shown in figure 11(*a*) and involves the following steps: (i) choose an arbitrary point 1*e* on the saturation boundary σ, with corresponding values $\hat{T}_\sigma$ and $\hat{P}_\sigma(\hat{T}_\sigma)$; (ii) to establish a Rayleigh line $\mathrm{R_e}$ for the equilibrium case and an initial state O, define the slope of the Rayleigh line as the arithmetic mean of the slopes of the single-phase and mixture isentropes at σ,

$$\left(\frac{\mathrm{d}P}{\mathrm{d}v}\right)_{\mathrm{R_e}} \equiv \frac{1}{2}\left[\left(\frac{\partial P}{\partial v}\right)_{\mathrm{s}}^{\mathrm{f}} + \left(\frac{\partial P}{\partial v}\right)_{\mathrm{s}}^{\mathrm{m}}\right], \tag{12}$$

this Rayleigh line defining an 'average' equilibrium shock system; (iii) construct a forward equilibrium-mixture adiabat and an inverse equilibrium-vapour adiabat

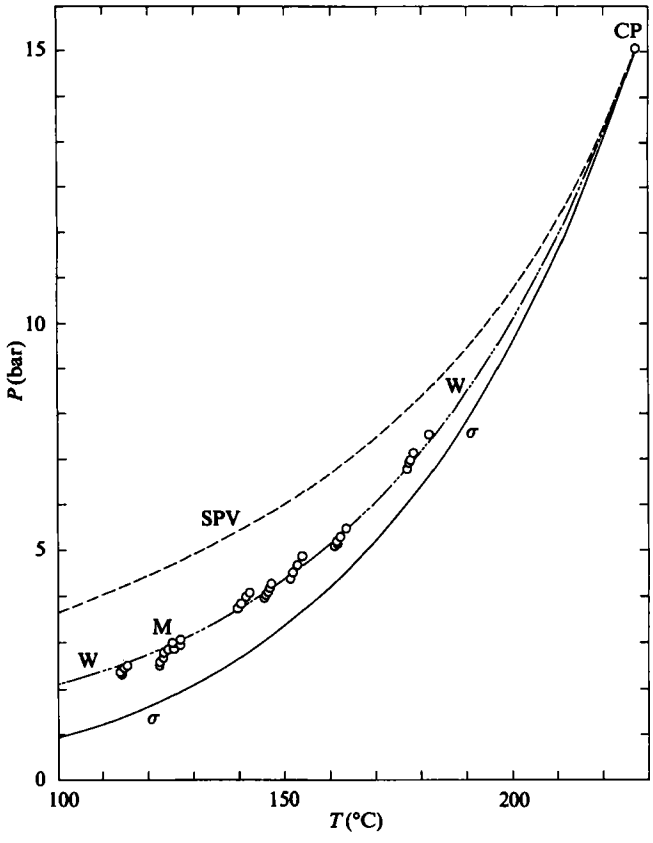

FIGURE 9. Pressure–temperature curve showing measured points of critical supersaturation and the corresponding Wilson line W for FC-75, using the Hobbs equation. SPV = vapour spinodal, CP = critical point. The cluster of data points labelled M represent a test for Mach-number independence of the critical supersaturation S_c, as described in figure 10.

from point 1*e*, the intersections of these adiabats with R_e defining the end state 2*e* and the common initial state 0, respectively; (iv) construct the forward vapour adiabat from point 0, the intersection of this adiabat with the Wilson line W fixing the point 1 for the non-equilibrium case and, thus, the slope of the corresponding Rayleigh line R; (v) continue the forward equilibrium-mixture adiabat to the intersection with R, thus defining the end state 2. These steps make use of the equality of slopes of the Rayleigh lines $0 \rightarrow 1$ and $1 \rightarrow 2$, corresponding to equal velocities of the forerunner shock and condensation discontinuity. For a given choice of point 1*e*, all states, in particular the pressures, are defined.

The results for FC-75 are shown in figure 11. The achievable pressure amplitudes (e.g. $P_2 - P_0$) are significantly greater in the non-equilibrium case, especially at lower pressures, where the supersaturation S_c can become quite large. The calculations described here do not represent maximum pressure amplitudes for a split-shock system; these may be significantly greater.

In unsteady-flow situations, in the shock-tube test section for example, the intermediate states 1 and 2 (see figure 1*b*) may be distributed and spatially non-uniform. The adiabat system is then more complex than shown in figure 7; in particular, the amplitudes of the discontinuities cannot be inferred from the shock adiabats alone.

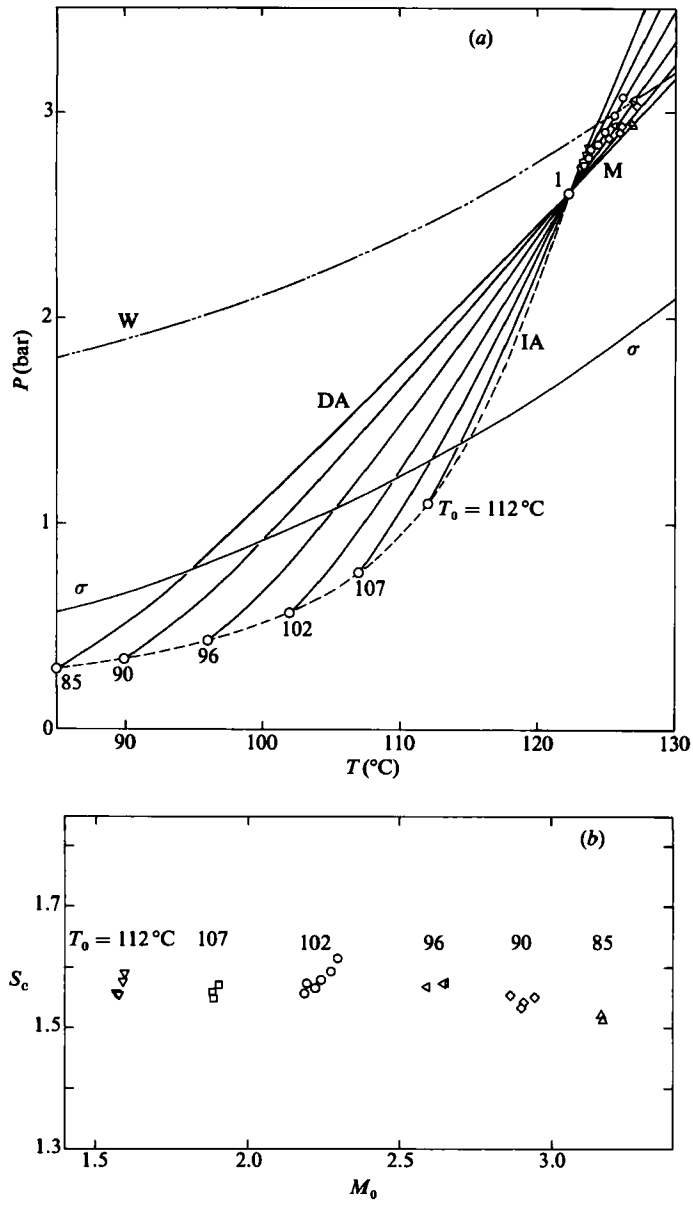

FIGURE 10. Experimental tests for uniqueness of a given state of critical supersaturation in FC-75. All calculations are based on the Hobbs equation of state. (*a*) Inverse shock adiabat in the pressure–temperature plane, for a fixed final state (estimated to be on the Wilson line), $P_1 = 2.61$ bar, $T_1 = 122$ °C. The data points show experimental initial states (○), and final states as follows: ▽, 112 °C; □, 107 °C; ○, 102 °C; <, 96 °C; ◇, 90 °C; △, 85 °C. (*b*) The experimental critical supersaturation S_c as a function of shock Mach number M_0, for initial temperatures T_0 between 85 °C and 112 °C. Symbol designations same as (*a*).

In the Rensselaer shock-tube experiments for which splitting was observed within the test section, the pressure amplitude of the condensation discontinuity was typically small, as already noted (Yoon 1985). In almost every case, the condensation discontinuity was overtaking the forerunner shock at the tube exit section.

2.2. *Shock-splitting experiments at the MPI, Göttingen*

These experiments were performed at moderate incident-shock (forerunner) Mach numbers, determined by the driver pressure and diaphragm selected. At low Mach numbers, the forerunner shock is not sufficiently strong to produce critical supersaturation and the vapour is only weakly supersaturated: in this case, condensation is delayed and the triple point is found by extrapolation. At higher Mach numbers, critical supersaturation is achieved and the triple point is determined by interpolation.

The experiments were performed in a shock tube with a conventional closed end. Depending on the diaphragm burst pressure and the initial state, splitting may occur in the incident-wave system or after reflection from the closed end. The various states for both incident-wave splitting and reflected-wave splitting are shown in figure 12.

The experimental set-up in the measurement section at the end of the Göttingen shock tube is shown in figure 13. The shock-tube inside diameter is 80 mm, the driver section is 2.50 m long and the test section 2.65 m long, measured from the diaphragm to the fixed endwall of the measurement section. The sidewalls of the measurement section are bored for the mounting of pressure transducers (Kistler 603B) and other probes. Two side windows of 12×180 mm permit a transverse view through the observation section close to the circular endwall. The entire length of the shock tube can be heated to about 180 °C. The tube is made of brass and the measurement section of stainless steel. A detailed description of the apparatus is given by Speckmann (1984).

Principal measurements were $P(t)$ from the Kistler 603B pressure transducers and light intensity $I(t)$ from the 'light gates', consisting of laser beams I_1 and I_2 directed at the respective photodiodes. The light gates and pressure transducers allow the measurement of both the forerunner-shock velocity U_{FS} and the condensation-discontinuity velocity U_{CD} (both considered to be in the laboratory frame). Temperature measurements were made in a few experiments.

Figure 14 shows two representative experiments for the determination of U_{FS} and U_{CD}. With a given set of initial conditions, the incident-shock Mach number M_s characterizes the experiment (with increasing strength, the incident shock may be a simple vapour-phase shock, a forerunner shock with trailing condensation discontinuity, or a liquefaction shock).

By plotting the experimental values of U_{FS} and U_{CD} against the shock Mach number, the triple point can be determined as the limit $U_{FS} = U_{CD}$, as shown in figure 15. The three branches of the shock-velocity curve correspond to the condensation discontinuity, forerunner shock, and at higher shock Mach number M_S, the combined liquefaction shock. The states shown in figure 15(*a*), for example, can be identified with the corresponding adiabats in figure 7(*a*). For M_S less than about 1.194 (the triple-point value), the U_{FS} curve corresponds to a shock Rayleigh line such as $0 \rightarrow e$ in figure 7(*a*); the triple point TP to a Rayleigh line such as $0 \rightarrow 1 \rightarrow 2$. For M_S greater than about 1.194, the (joined) U_{LS} curve corresponds to a Rayleigh line such as $0 \rightarrow l$. The shock Mach number corresponding to equilibrium saturation σ was calculated from the BWR44 equation of state (Yamada 1973). Critical-supersaturation data derived from plots similar to figure 15 determine a Wilson line for a given test fluid.

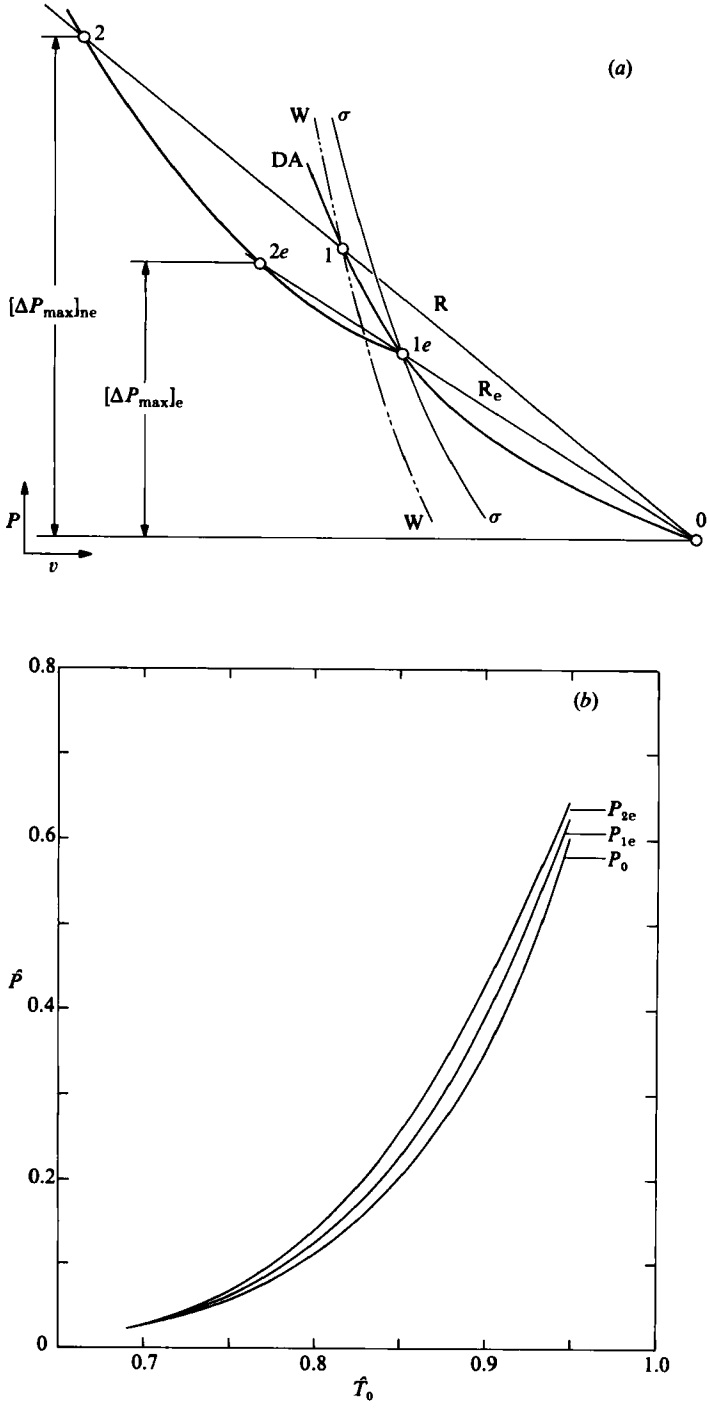

FIGURE 11 (*a*, *b*). For caption see facing page.

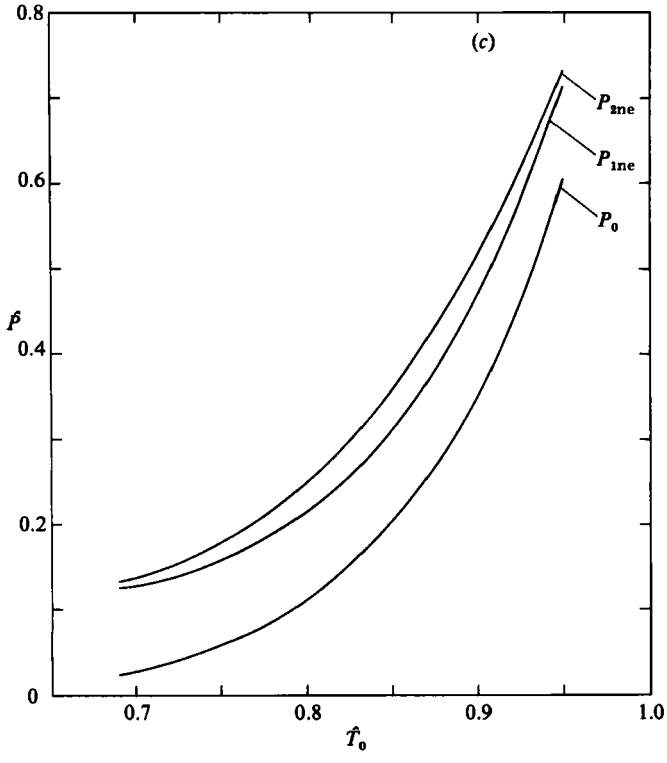

FIGURE 11. Pressure amplitudes corresponding to a triple point for equilibrium and non-equilibrium shock splitting. (*a*) Sketch showing the defined construction in the pressure–volume plane for the triple-point pressures P_0, P_1 and P_2. (*b*) Equilibrium pressure amplitudes for FC-75 as a function of reduced temperature $\hat{T}_0$. (*c*) Non-equilibrium pressure amplitudes for FC-75 as a function of reduced temperature $\hat{T}_0$. (*c*) Non-equilibrium pressure amplitudes for FC-75 as a function of reduced temperature $\hat{T}_0$.

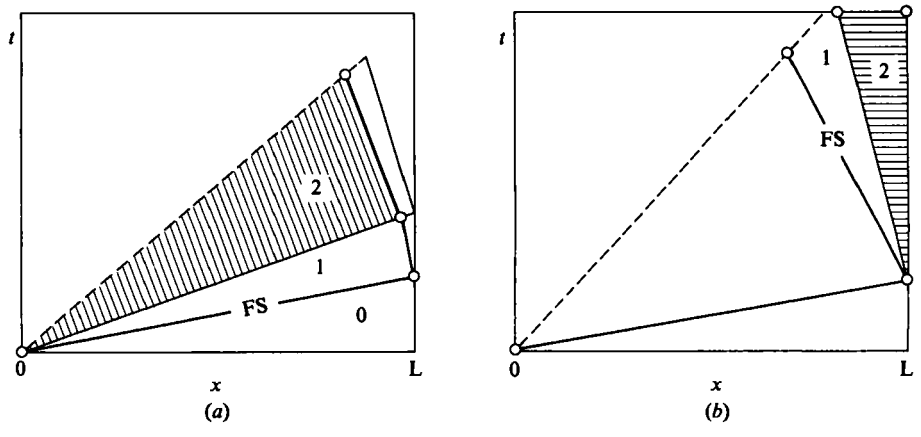

FIGURE 12. Schematic wave diagrams in (x, t) coordinates, showing the state designations for the MPI shock-splitting experiments. Shaded regions indicate mixture states 2. State 1 corresponds to metastable vapour. (*a*) Shock splitting in the incident wave. (*b*) Shock splitting in the reflected wave.

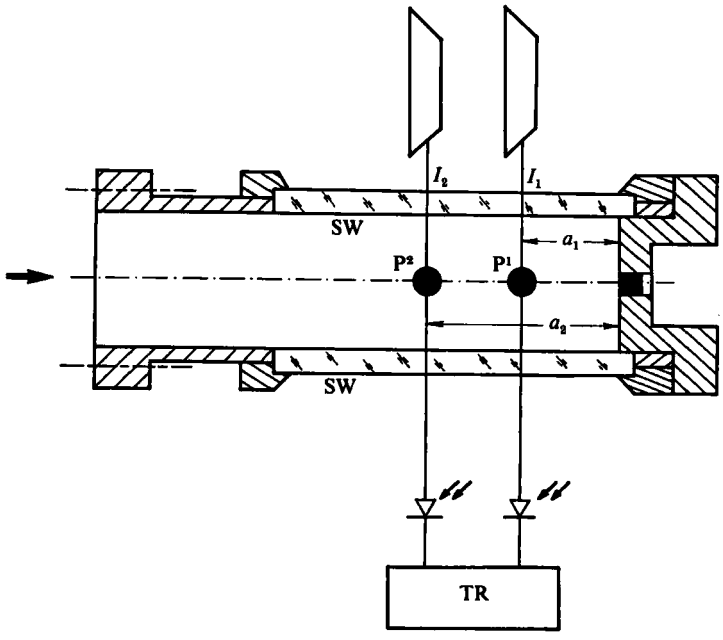

FIGURE 13. Measurement section at the end of the MPI shock-tube test section. The dimensions a_1 and a_2 are the distances of the laser beams I_1 and I_2 from the endwall and the distances of the pressure transducers P^1 and P^2 which are exactly aligned with the laser beams. The arrow indicates the propagation direction of the incident shock. Double arrows indicate the photodiodes. SW = side window. TR = transient recorder.

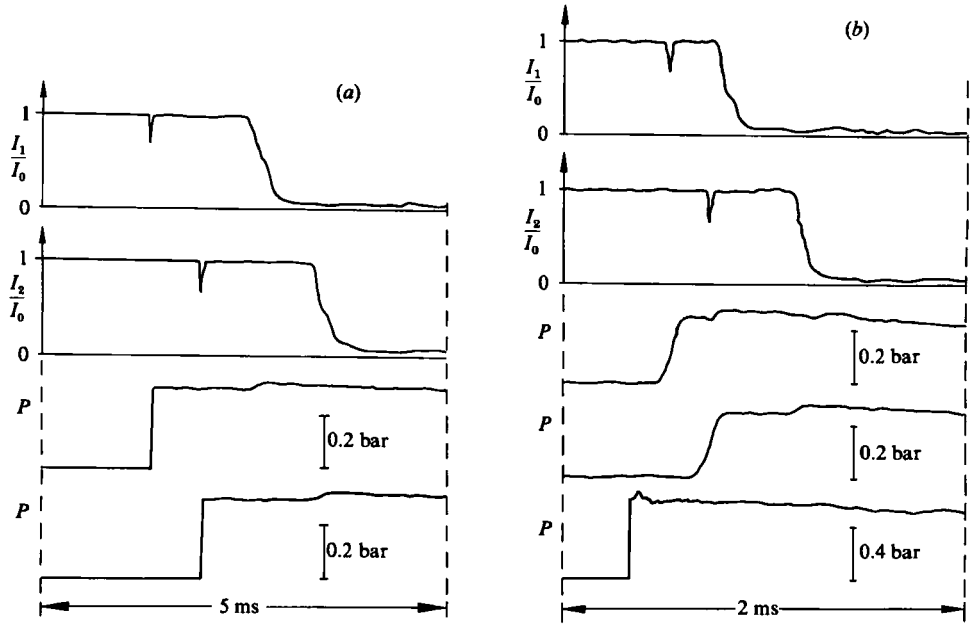

FIGURE 14. Light-gate transmitted intensity I and pressure P as functions of time at the measuring stations a_1 and a_2, showing the arrival of the forerunner shock (intensity blip and step rise in pressure) and the later arrival of the condensation discontinuity (intensity fall and small-step rise in pressure). (*a*) Splitting in the reflected wave in test fluid PP3, initial conditions $T_0 = 60$ °C, $P_0 = 0.70$ bar; $a_1 = 116$ mm, $a_2 = 216$ mm. (*b*) Splitting in the reflected wave system in test fluid PP3, initial conditions $T_0 = 130$ °C, $P_0 = 0.67$ bar; $a_1 = 50$ mm, $a_2 = 100$ mm; the bottom pressure trace is from the endwall pressure transducer.

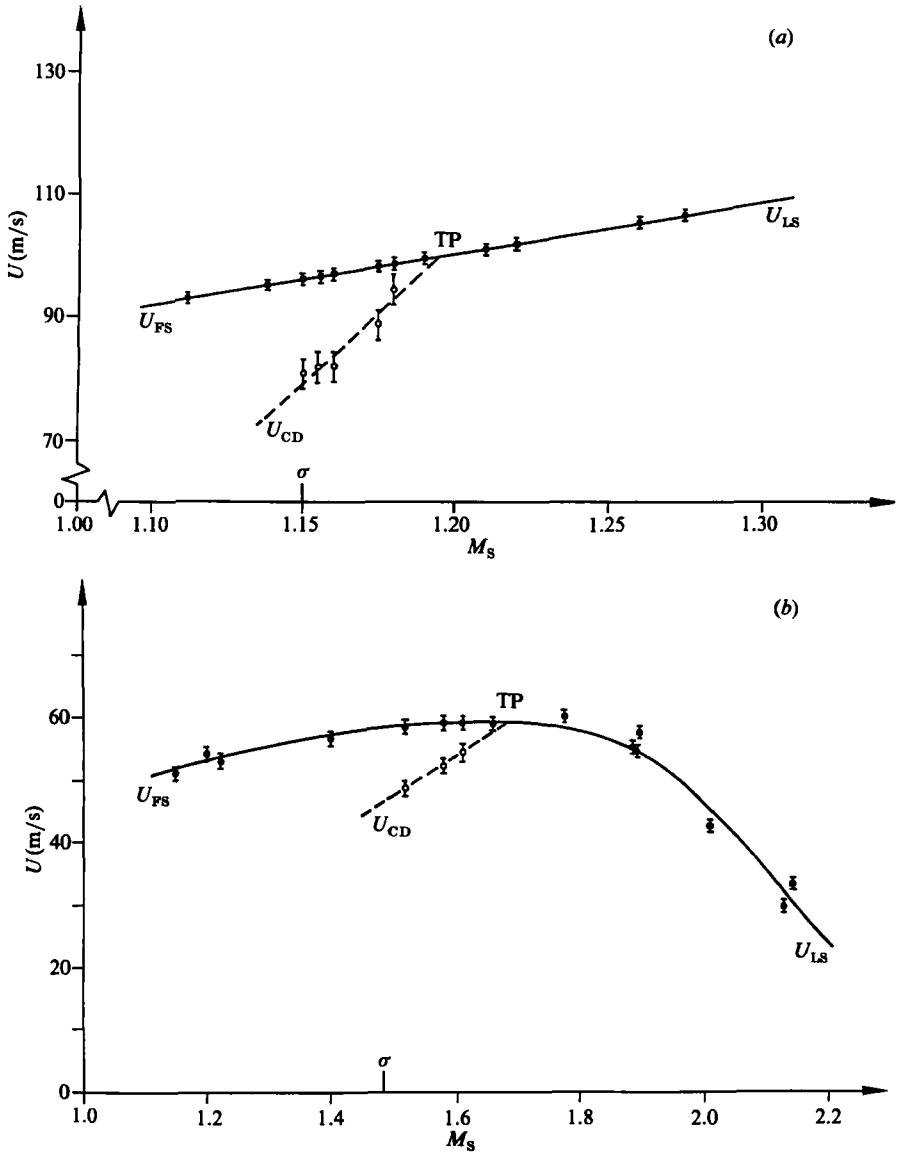

FIGURE 15. Velocity of the forerunner shock U_{FS}, condensation discontinuity U_{CD} and combined liquefaction shock U_{LS} as a function of incident-shock Mach number M_S. The intersection of U_{CD} and U_{FS} determines the triple point TP, corresponding to critical supersaturation. The value of M_S at which saturation is achieved (after reflection, in the case of splitting in the reflected-wave system) is indicated by the symbol σ. FS = forerunner shock, CD = condensation discontinuity, LS = liquefaction shock. (*a*) Incident-wave splitting in the fluorocarbon PP3, $T_0 = 100$ °C, $P_0 = 0.90$ bar. (*b*) Reflected-wave splitting in the fluorocarbon PP3, $T_0 = 130$ °C, $P_0 = 0.67$ bar.

2.3. *On the mechanism of coalescence and splitting*

The interaction of acoustic waves with the forerunner shock and the subsonic condensation discontinuity provides a mechanism for the coalescence of a split-wave system into a liquefaction shock, or for the splitting of an existing liquefaction shock. Suppose, for example, that a split-wave system is being driven from behind by an

accelerating piston (see figure 1*b*). The compression waves from the piston pass through the condensation discontinuity CD and strengthen the forerunner shock FS: this increases the supersaturation behind it and the condensation discontinuity is then accelerated by the increased nucleation rate, leading to coalescence (note that the increase in the velocity of the CD exceeds the increase in the velocity of the FS – see e.g. figure 15*a*). Similarly, a liquefaction shock can be weakened by rarefaction waves from behind: when it becomes sufficiently weak that critical supersaturation is no longer reached within the shock front, it will split.

3. Liquid-evaporation wave splitting

The splitting of a pressure-release wave travelling through a liquid has already been described in §1 and illustrated in figures 1, 2 and 3. The experiments described here were performed at the MPI, Göttingen (Chaves 1980, 1984).

The observations were carried out in the expansion tube shown in figure 16. The rectangular test section is 110 mm long and approximately 20×15 mm in cross-section, with front and back walls of optical glass (i.e. windows in the plane of figure 16) so that the flow within can be optically observed. (For experiments in test sections of non-constant cross-section, see Chaves 1984, Puttendörfer 1982 and Meier & Thompson 1985.) The sidewalls are bored for the mounting of pressure transducers (Kistler 603B); alternatively, the pressure transducers may be replaced by thermocouples or blank inserts.

In a typical experiment, the expansion tube is fitted with a diaphragm (hardened aluminium in a thickness range 0.1–0.2 mm), evacuated, then partially filled with test liquid and heated to the required initial temperature. The test section then contains equilibrium saturated liquid in the lower part and saturated vapour above, both at the vapour pressure $P_\sigma(T)$. The heating of the test section is accomplished by an enclosing shroud with hot-air circulation, allowing test temperatures up to 200 °C.

The diaphragm D is ruptured by the release of a piercing arrow device A, driven by a stretched spring. The arrow is held in the 'loaded' position by an electromagnet which is switched off to initiate the experiment. The rupture of the diaphragm opens the test section to the large vacuum vessel V above (2 m long × 240 mm diameter). Expansion waves travelling into the fluid then produce an upward flow into the vacuum vessel. The essential measurements in the test section are the initial parameters P_0 and T_0, the pressure $P(t)$ at several transducer locations and the liquid or mixture density measurement, based on intensity measurements of partial reflection of an oblique laser beam from the test-section window (see figure 16*b*).

The test fluid in the experiments reported here is PP1 (perfluoro-*n*-hexane). The critical temperature 177.9 °C (additional properties are given in Φ).

3.1. *Experimental observations of the splitting into a forerunner wave and an evaporation wave*

After diaphragm rupture, an expansion (pressure-release) wave propagates downward into the test section. This wave splits into two distinct waves, as shown by the pressure records; we shall call these two waves the forerunner wave FW and evaporation wave EW, consistent with the description in §1. The system of adiabats is shown in figure 17. The initial liquid state 0 lies on the saturation boundary σ. The forerunner wave is a simple acoustic expansion wave which brings the liquid to the supersaturated state 1 on the metastable isentrope. Strictly speaking, this forerunner wave is subject to classical spreading characterized by the parameter $\Gamma/\rho c$. For

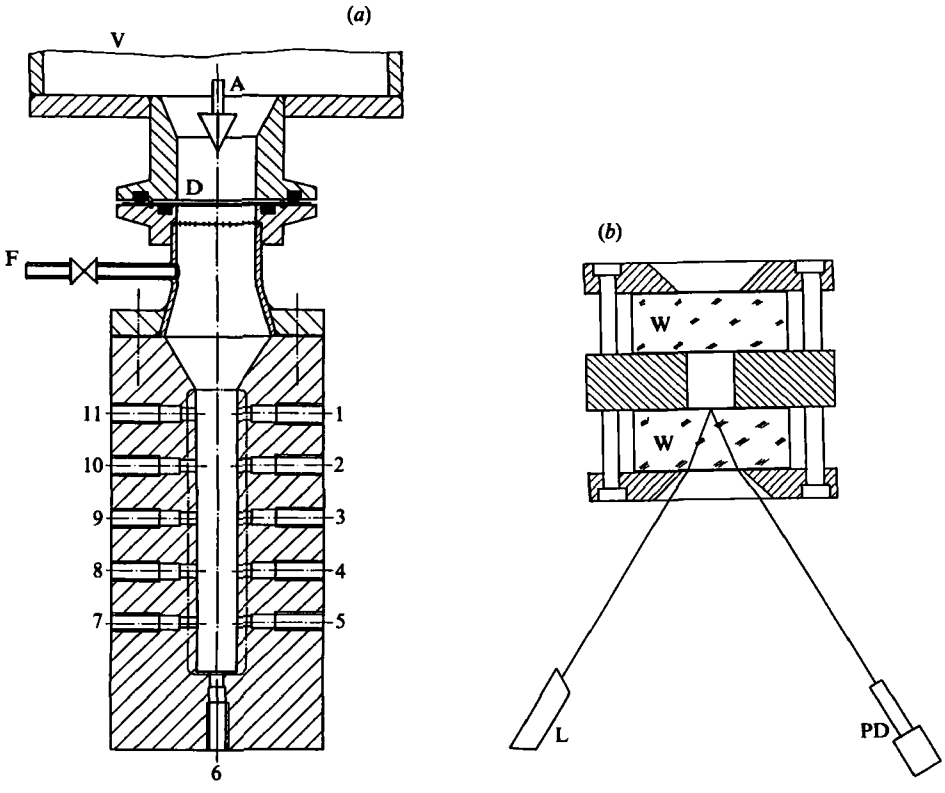

FIGURE 16. MPI expansion tube. (*a*) Axial cut through the test section, vacuum vessel V, diaphragm section D, filling or evacuation tube F and diaphragm-piercing arrow A. Transducer locations are numbered 1–11. (*b*) Cross-section through the test section, showing the front and back glass windows W and indicating the density-measurement technique with laser L and photodiode PD.

liquids, however, this parameter has a small value compared to that of gases; the value for liquid water at STP is about 10^{-3} of that for air at STP, for example. It is thus not surprising that no spreading of the forerunner wave is observed in our small-scale experiments – the forerunner wave can indeed be characterized as a discontinuity, which propagates with the local liquid soundspeed. At higher temperatures, the nucleation rate in the supersaturated state 1 behind the forerunner wave is sufficiently high to produce rapid evaporation, leading to an evaporation wave with a propagation velocity that is limited by the Chapman–Jouguet (sonic outflow) condition, as in classical deflagration, thus defining the two-phase equilibrium state 2 behind the evaporation wave, as illustrated in figure 17. States 0 and 2 then lie on a common deflagration adiabat (which has small departure from the equilibrium isentrope passing through 0). The evaporation-wave propagation velocity, limited by a gasdynamic condition, is thus similar to that of the mixture-evaporation shock described in Φ and illustrated in figure 3, but unlike that of the condensation discontinuity in shock splitting.

The location of state 2 and the extent to which it satisfies the Chapman–Jouguet condition is experimentally established by the (redundant) measurements of the pressures P_1 and P_2, the density ρ_2 and the wave velocity U_{EW} of the evaporation wave. These measurements were compared with the calculated Chapman–Jouguet state, based on the Abbott equation of state (Abbott 1973; Chaves 1980).

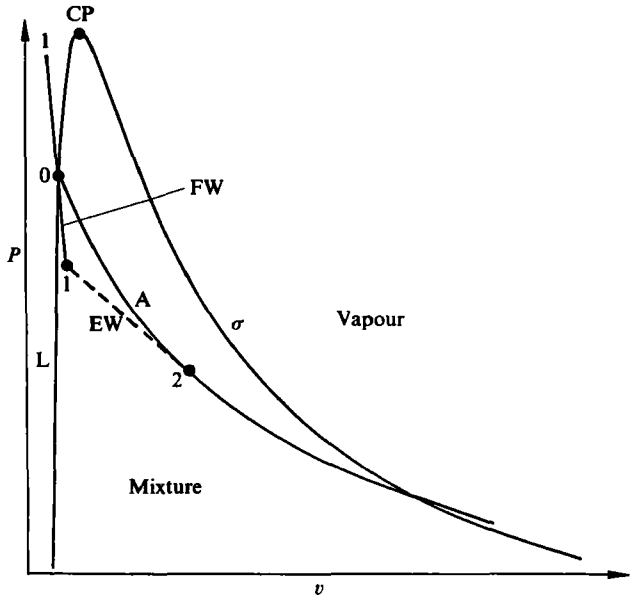

FIGURE 17. Pressure–volume diagram for liquid-evaporation wave splitting in the test section. CP = critical point, L = liquid isentrope passing through the initial state 0, A = deflagration adiabat through state 0, FW = forerunner wave, EW = evaporation wave. State 1 is a metastable-liquid state; state 2 is shown satifying the Chapman–Jouguet condition.

Experimental pressure records are shown in figure 18. In figure 18(*a*), the pressure signals $P(t)$ from transducers 1–6 are vertically separated in uniform steps so that the figure is similar to a wave diagram, with distance X on the vertical coordinate and time t on the horizontal. The path of the forerunner wave FW and its reflection from the closed bottom of the tube can be observed, as well as the path of the evaporation wave EW and its reflection EWR (for a proper and detailed wave diagram, see Chaves 1984). The states between EW and EWR correspond to the Chapman–Jouguet state 2. One can infer from figure 18(*a*) that the evaporation wave is triggered by the arrival of the reflected forerunner wave at the free surface. Diaphragm burst occurs at $t \approx 5$ ms in this experiment. Prior to burst, small-amplitude pressure oscillations result from the downward displacement of the diaphragm from the force of the (already activated) arrow A. This displacement produces weak pressure waves in the fluid. In figure 18(*b*) the wave splitting can also be observed, but is not quite so distinct at the lower temperature. The amplitude of the forerunner wave is considerably greater.

Figure 19 shows experimental and theoretical values of the wave propagation velocity for both the forerunner wave and the evaporation wave. The theoretical value of the forerunner velocity is simply the liquid sound speed $(\partial P/\partial \rho)_s^{\frac{1}{2}}$; the evaporation-wave velocity calculation assumes a Chapman–Jouguet condition and is found from the slope of the Rayleigh line $1 \rightarrow 2$:

$$U_{\mathrm{EW}} = V_1 \left[\frac{P_1 - P_2}{V_2 - V_1}\right]^{\frac{1}{2}}, \tag{13}$$

where $P_1(T_0)$ is a smoothed experimental value and the remaining properties are calculated from the Abbott equation of state.

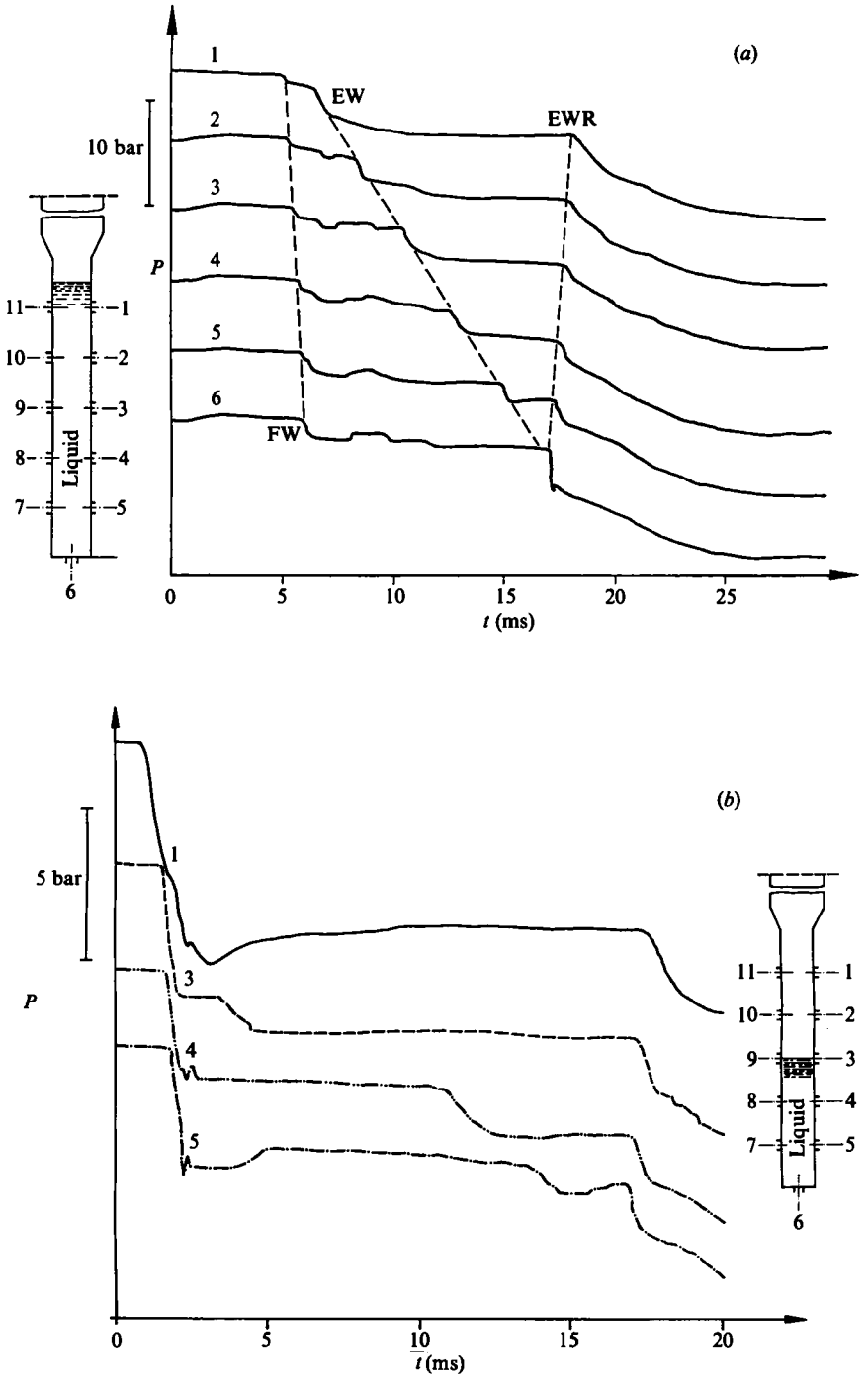

FIGURE 18. Pressure $P(t)$ from the numbered transducers along the length of the tube test section. The initial pressures are all equal to P_0. (*a*) $T_0 = 165$ °C, $P_0 = 14.7$ bar. Pressure traces are vertically separated. FW = forerunner wave, EW = evaporation wave, EWR = reflected evaporation wave. (*b*) $T_0 = 155$ °C, $P_0 = 12.3$ bar.

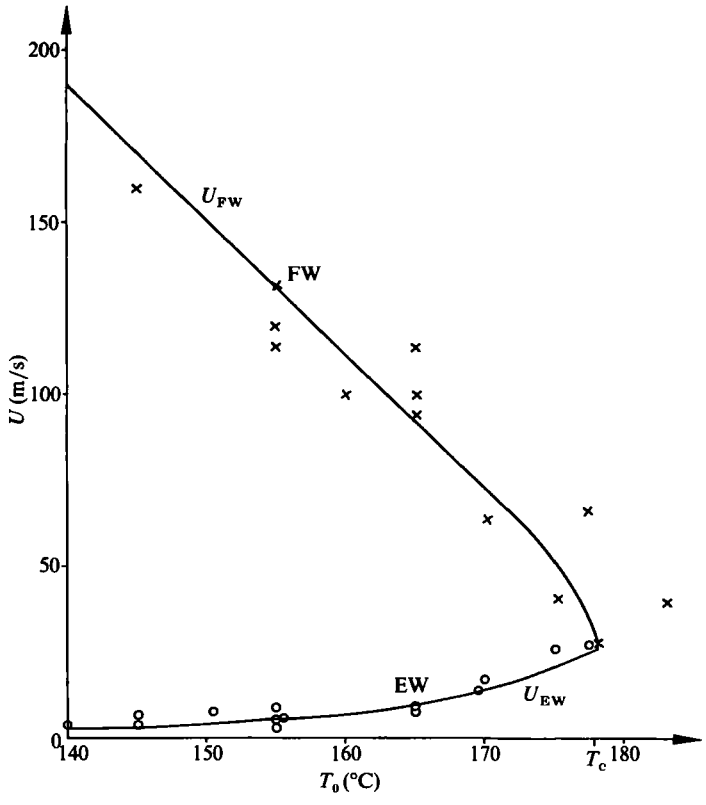

FIGURE 19. Propagation velocity U_{FW} of the forerunner wave (FW) in the liquid and of the evaporation wave (EW) as functions of the initial temperature T_0. The solid curve for U_{FW} is the calculated speed of sound in the liquid. The solid curve U_{EW} is calculated from equation (13).

Figure 20 shows the pressure amplitude of the forerunner wave and the evaporation wave compared to simple theoretical models. The experimental, normalized forerunner amplitudes in figure 20(*a*) are compared to curves of constant nucleation rate $J(T_0, \Delta P)$. At higher initial temperatures ($T_0 \geqslant 150°$ C, say) the curves of constant nucleation rate are nearly coincident with the pressure-amplitude data: this implies that the pressure P_1 falls until the nucleation rate becomes large enough to generate an opposing compression in the liquid. At lower initial temperatures, nucleation is no longer controlling and the amplitude data depart from the constant-nucleation-rate curves. The amplitude curves for the evaporation wave in figure 20(*b*) are calculated on the same basis as the evaporation-wave velocity.

The successive photographs of the forerunner wavefront shown in figure 21 show a structure reminiscent of the 'fingering' observed in certain accelerating flame fronts. The motion-picture frames, made in 1977 at MPI, show a forerunner wavefront in PP3 test substance, with nucleation behind the front. This interpretation is based on the propagation velocity of 150 m/s measured from the frames, corresponding almost exactly to the liquid sound speed at the experimental temperature. More definitive experiments are clearly needed.

It is of interest to compare the evaporation rates across the evaporation wavefront with those achieved in 'vapour explosions', i.e. the sudden explosion of a liquid droplet heated nearly to the spinodal limit in a bubble column experiment

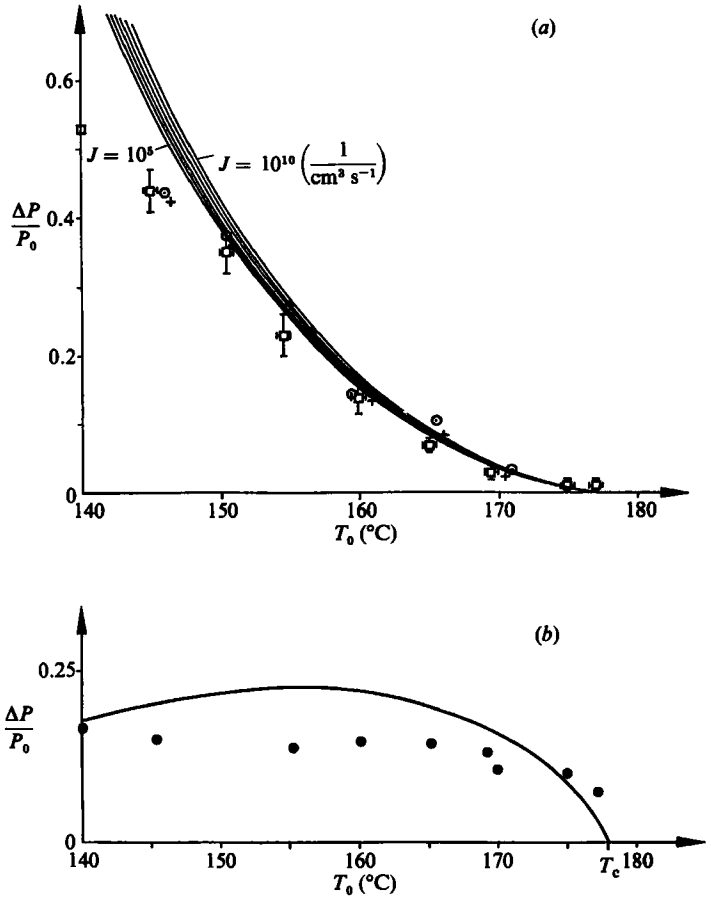

FIGURE 20. Normalized pressure amplitude ΔP of the forerunner wave and the evaporation wave as a function of initial temperature T_0. The pressure is normalized by the initial pressure P_0. (*a*) Forerunner-wave amplitude data compared to lines of constant nucleation rate. Data of Puttendörfer (1982) (+ and ⊙) and Chaves (1984) (□). (*b*) Evaporation-wave amplitude data and theoretical curve calculated on the same basis as equation (13).

(Shepherd & Sturtevant 1982). A typical value reported by these authors for butane-droplet explosions is 400 (g/cm^2) s^{-1}. In our experiments, with $\rho \sim 1.6$ g/cm^3, $U_{EW} \approx 10^3$ cm/s (see figure 19) and a downstream moisture fraction of $y \sim 50\,\%$, the evaporation rate per unit area of surface is $\approx (1.6)\,(10^3)\,(0.5) = 800$ (g/cm^2) s^{-1}. Thus, with a density ratio of PP1 to butane of 2:1, the liquid volumetric evaporation rate is about the same.

4. Concluding remarks

Wave splitting in adiabatic vapour-condensation systems shows remarkable parallels to wave splitting in adiabatic liquid-evaporation systems. Both phenomena show splitting into pressure waves and following phase-change waves, which convert a metastable, nominally single-phase state into a mixture. In the case of condensation, the velocity of the phase-change wave appears to be governed by nucleation and droplet growth; in the case of liquid evaporation, the velocity of the

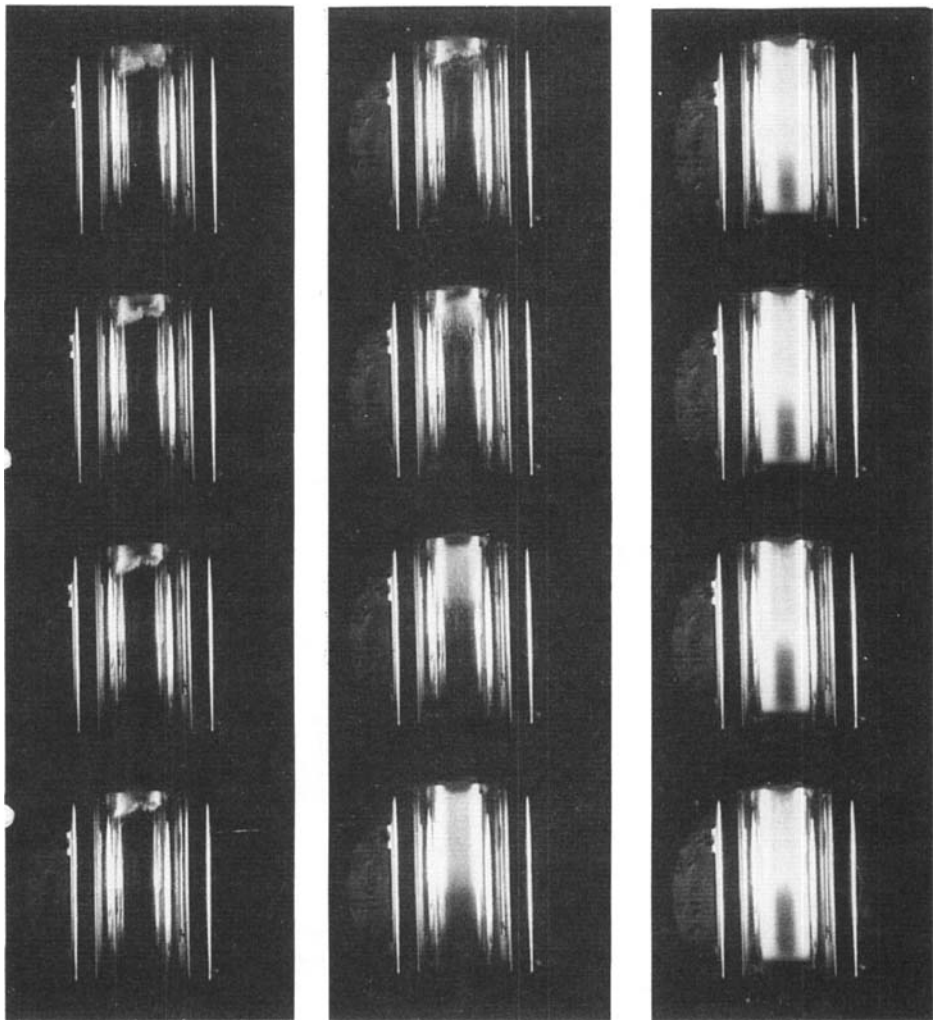

FIGURE 21. Photographs of the forerunner wavefront propagating downward in the test section. Test fluid PP3, $T_0 = 210$ °C, $P_0 = 14$ bar. The fluid above the wavefront is a liquid with numerous nuclei. The fluid below, i.e. ahead of the wave, is undisturbed liquid. The forerunner wave originates from the top in frame 5, corresponding approximately to the first rarefaction wave from the diaphragm burst above. The time interval between frames is 0.13 ms.

phase-change wave appears to be governed by the Chapman–Jouguet condition for deflagration.

The important role of nucleation has been described here only superficially. The sound speeds in the metastable, supersaturated states have been conveniently treated as though no nucleation were occurring, i.e. a single-phase state, in particular for the case of vapour-side shock splitting. A realistic physical model would require coupling of the flow and nucleation dynamics (see e.g. Dobbins 1983) and some description of the corresponding dispersive sound speed.

It is a pleasure to acknowledge the assistance of Esther Parslow Rendano in the preparation of the manuscript. Especially helpful were discussions with N. Kerls.

Partial support for travel was provided under National Science Foundation Grant INT-8214100. The research at Rensselaer was supported by NSF Grant MSM-8412849.

Note added in proof: It has been pointed out by Dr E. Zanner that observations of a liquid-evaporation wave were reported by Grolmes & Fauske in 1974 (*Proc. Fifth Intl. Heat Transfer Conf., Vol.* 4, pp. 30–34). Cf. §3.1 of this paper.

REFERENCES

ABBOTT, M. M. 1973 Cubic equations of state. *AIChE. J.* **19**, 596–601.

BETHE, H. A. 1942 The theory of shock waves for an arbitrary equation of state. *Rep.* 545, p. 57. *Office of Scientific Research and Development*, Washington.

CHAVES, H. 1980 Verdampfungswellen in retrograden Flüssigkeiten. Diplomarbeit, Georg-August-Universität. Göttingen.

CHAVES, H. 1984 Phasenübergänge und Wellen bei der Entspannung von Fluiden hoher spezifischer Wäerme. Dissertation, Georg-August-Universität. Göttingen.

CHAVES, H., LANG, H., MEIER, G. E. A. & SPECKMANN, H.-D. 1985 Adiabatic phase transitions and wavesplitting in fluids of high specific heat. In *Flow of Real Fluids* (ed. G. E. A. Meier & F. Obermeier). Lecture Notes in Physics, vol. 235, pp. 115–124. Springer.

DETTLEFF, G., MEIER, G. E. A., SPECKMANN, H.-D., THOMPSON, P. A. & YOON, C. 1982 Experiments in shock liquefaction. In *Proc. 13th Intl Symp. on Shock Tubes and Waves* (ed. C. E. Trainor & J. G. Hall), pp. 616–623. State University of New York Press, Albany.

DETTLEFF, G., THOMPSON, P. A., MEIER, G. E. A. & SPECKMANN, H.-D. 1979 An experimental study of liquefaction shock waves. *J. Fluid Mech.* **95**, 279–304.

DOBBINS, R. A. 1983 A theory of the Wilson line for steam at low pressures. *Trans. ASME* I: *J. Fluids Engng* **105**, 414–422.

ERMAKOV, G. V. & SKRIPOV, V. P. 1968 Experimental determination of the specific volumes of a superheated liquid. *High Temperature* **6**, 86–92.

GUST, W. H. & YOUNG, D. A. 1979 *High Pressure Science and Technology* (ed. K. D. Timmerhaus & M. S. Barber), vol. I, pp. 944–952. Plenum.

HAYES, W. D. 1958 The basic theory of gasdynamic discontinuities. In *Fundamentals of Gasdynamics* (ed. H. W. Emmons), pp. 416–481. Princeton University Press.

HOBBS, D. E. 1983 A virial equation of state utilizing the principle of corresponding states. Dissertation, Rensselaer Polytechnic Institute.

LIEPMANN, H. W. & LAGUNA, G. A. 1984 Nonlinear interactions in the fluid mechanics of helium II. *Ann. Rev. Fluid Mech.* **16**, 139–178.

LIGHTHILL, M. J. 1956 Viscosity effects in sound waves of finite amplitude. In *Surveys in Mechanics* (ed. G. K. Batchelor & R. M. Davis), pp. 250–351. Cambridge University Press.

MCQUEEN, R. G. & MARSH, S. P. 1968 Hugoniots of graphites of various initial densities and the equation of state of carbon. In *Behavior of Dense Media under High Dynamic Pressures*, pp. 207–216. Gordon and Breach.

MEIER, G. E. A. & THOMPSON, P. A. 1985 Real gas dynamics of fluids with high specific heat. In *Flow of Real Fluids* (ed. G. E. A. Meier & F. Obermeier). Lecture Notes in Physics, vol. 235, pp. 103–114. Springer.

MIHALAS, D. & MIHALAS, B. W. 1984 *Foundations of Radiation Hydrodynamics*, pp. 611–649. Oxford University Press.

PUTTENDÖRFER, E. 1982 Schallnahe Strömung eines retrograden Fluides. Diplomarbeit, Georg-August-Universität, Göttingen.

SHEPHERD, J. E. & STURTEVANT, B. 1982 Rapid evaporation at the superheat limit. *J. Fluid Mech.* **121**, 379–402.

SMITH, J. A. 1968 Experimentally determined of the shock reflection process in ionizing xenon. *Phys. Fluids* **11**, 2150–2161.

SPECKMANN, H.-D. 1984 Aufspaltung von Kondensationsstosswellen in Fluiden höher spezifischer Wärme. Dissertation, Georg-August-Universität, Göttingen.

THOMPSON, P. A. 1972 *Compressible-Fluid Dynamics*, pp. 315–326. McGraw-Hill.

THOMPSON, P. A. 1983 Shock-wave series for real fluids. *Phys. Fluids* **26**, 3471–3474.

THOMPSON, P. A., CAROFANO, G. C. & KIM, Y.-G. 1986 Shock waves and phase changes in a large-heat-capacity fluid emerging from a tube. *J. Fluid Mech.* **166**, 57–92.

THOMPSON, P. A. & KIM, Y.-G. 1983 Direct observation of shock splitting in a vapor-liquid system. *Phys. Fluids* **26**, 3211–3215.

THOMPSON, P. A., KIM, Y.-G. & MEIER, G. E. A. 1984 Shock tube studies with incident liquefaction shocks. In *Proc. 14th Intl Symp. on Shock Tubes and Waves* (ed. R. D. Archer & B. E. Milton), pp. 413–420. New South Wales University Press, Sydney.

WEGENER, P. P. & WU, B. J. C. 1977 Gasdynamics and homogeneous nucleation. *Adv. Colloid Interface Sci.* **7**, 325–417.

WONG, H. & BERSHADER, D. 1966 Thermal equilibration behind an ionizing shock. *J. Fluid Mech.* **26**, 459–479.

YAMADA, T. 1973 An improved generalizated equation of state. *AIChE. J.* **19**, 286–291.

YOON, C. 1985 Incident-shock liquefaction experiments with retrograde substances. Dissertation, Rensselaer Polytechnic Institute.

ZEL'DOVICH, YA. B. & RAIZER, YU. P. 1967 *Physics of Shock Waves and High-Temperature Hydrodynamic Phenomena*, vol. 2 (ed. W. D. Hayes & R. F. Probstein), pp. 750–756. Academic.